Density Functional Theory Applied to Structure and Vibrational Band Analysis of an Aggregated Thiacarbocyanine

Metin Aydin, Fleumingue Jean-Mary, Nathan Stevens, and Daniel L. Akins*

Center for Analysis of Structures and Interfaces (CASI), Department of Chemistry, The City College of The City University of New York, New York, New York 10031

Received: December 2, 2003; In Final Form: March 4, 2004

Density functional theory at the B3LYP level, using the 6-31G(d) basis set, was employed to calculate structural properties (e.g., bond distances, bond angles, charge distributions, and Raman vibrational frequencies) for isolated single molecules of the cyanine dye 3,3′-diethyl-5,5′-dichloro-9-benzothiacarbocyanine (hereinafter referred to as DDPT). Calculations indicate that there are two favorable ground-state equilibrium structures: the more-stable structure is near planar, with a 14.4° twist between the two benzothiazole moieties, whereas the other structure lies 107 cm^{-1} above it and is planar. For the two structures, calculations indicate that the methyl groups of the ethyl substituents lie on the same side of the structural surface of the macrocycle, opposite to the phenyl ring on the methane bridge, and the phenyl ring makes an angle of 83.4° and 89.7° with the near-planar and planar conformers, respectively. We further have observed that, with nonresonant excitation for aggregated DDPT, changes in the Raman band intensity indicate that aggregation results in enhanced scattering for bands composed of vibrational modes that contain major contributions from in-plane skeletal deformations of the benzothiazole moieties, as well as vibrations involving the phenyl ring and the trimethine bridge. With resonant excitation of the aggregate, two new Raman bands in the low-frequency region (at 142 and 161 cm^{-1}) appear, as well as other bands that are associated with out-of-plane distortions of the benzothiazole moieties and the phenyl ring. Our findings are discussed in terms of Albrecht's *A* and *B* terms, and we utilize information concerning active vibrational motions to aid in deciphering how monomers are arranged within the aggregate structure.

I. Introduction

Research that involves understanding the structure and optical properties of molecular aggregates that are formed through the noncovalent self-assembly of molecules has garnered significant attention, because such information may provide (i) models for investigating intermolecular interactions between molecules in other systems, (ii) the prospect of gaining insight about the optical and population dynamics for small grouping of molecules, and (iii) the utilization of molecular aggregate structures as the functional elements for device and chemical sensor applications. Some key studies in the literature concerning aggregated molecules as model systems have focused on charge-separation steps in photosynthesis,[1−4] spectral sensitization,[5] photoconduction,[6] optical probes in biological and synthetic membrane systems,[7] and nonlinear optical materials.[8−10]

Simplified, and widely used, structural models for aggregates that seem to identify the important interactions between monomers within the extended structure are the so-called J- and H-aggregate spatial alignments. These alignment structures, i.e., the J- and H-aggregates, are defined by the relative orientations of induced transition dipole moments of the constituent monomers, either "head-to-tail" or "head-to-head," respectively. The absorption spectra for J- and H-type aggregates are red- and blue-shifted, respectively, relative to that of the absorption band of the monomer, and the optical dynamics of such aggregates differs substantially from that of the monomer as well. In this paper, the structure of aggregated 3,3′-diethyl-5,5′-dichloro-9-benzothiacarbocyanine (hereinafter referred to as DDPT) is investigated. Experimental techniques utilized in this study include ultraviolet−visible (UV−Vis) absorption, emission, and Raman spectral measurements. Also, density functional theory (DFT) at the B3LYP level, using the 6-31G(d) basis set, has been employed to calculate bond distances, bond angles, charge distributions, and Raman vibrational frequencies for isolated single molecules of DDPT. The present study is a continuation of efforts to couple structural theory and spectroscopic methods to gain insight into molecular aggregate structure, similar to that provided by an earlier quantum chemical investigation for pseudo-isocyanine (PIC) that was reported by this laboratory.[11]

II. Experimental System and Computational Methods

Experimental Section. All spectroscopic measurements were conducted at room temperature. DDPT was purchased from the Japanese Research Institute for Photosensitizing Dyes, Ltd. (Okayama, Japan) and used without further purification. Two stock solutions of DDPT were prepared: one with the chloride salt of DDPT dissolved in high-performance liquid chromatography (HPLC)-grade methanol as the solvent, to prepare a solution with a concentration of $\sim 1 \times 10^{-3}$ M, and another that consisted of the chloride salt dissolved in distilled water to form a solution with a concentration of $\sim 2.5 \times 10^{-4}$ M. We also prepared a colloidal silver sol, according to the method of Creighton et al.,[12] with slight modification.

The UV−Vis spectrum of DDPT in an aqueous solvent is shown in Figure 1. Raman spectroscopic studies were conducted

* Author to whom correspondence should be addressed. Telephone: 212-650-6953, ext. 6023, 7111, 8428. Fax: 212-650-6848. E-mail address: akins@scisun.sci.ccny.cuny.edu.

10.1021/jp037678w CCC: $27.50
Published on Web 06/09/2004

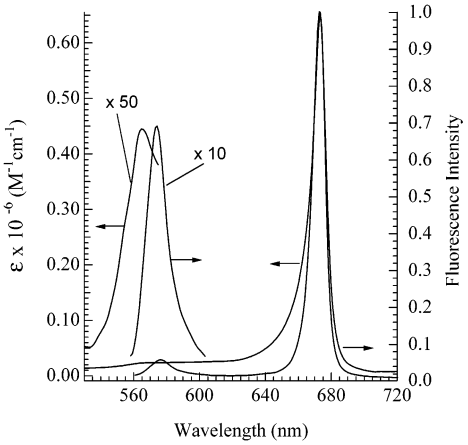

Figure 1. Absorption and fluorescence spectra of 10^{-5} M DDPT in water. Scale factors for enhancement of signals for weak bands are indicated by the numbers that are tagged to the curves. (Spectra taken from an earlier paper published by author D.L.A. (Özçelik, S.; Akins, D. L. *J. Phys. Chem. B* **1999**, *103*, 8926).)

using a 1:1 volume ratio of the aqueous stock solution (ca. 2.5 $\times$ 10^{-4} M) and the silver colloid solution (ca. 1 $\times$ 10^{-4} M), which was placed in a 1-cm quartz cuvette. The purpose of the silver colloid (i.e., silver sol) was to facilitate aggregation of DDPT, which occurs on the sol particle's surface. For aggregated molecules, surface-enhanced Raman scattering (SERS) has been shown, through many investigations in the author's laboratory,[11] to have essentially no role in the enhancement or the relative intensities of Raman bands when aggregation-enhanced Raman scattering (i.e., AERS; see below) is operative. Consequently, because AERS is the enhancement mechanism that our studies have shown to be applicable here (see below), no measurable SERS modification of relative Raman band intensities occurs.

For nonresonant excited Raman spectra of DDPT in the homogeneous methanol solution and the mixed aqueous colloidal systems, the 705 nm line (of a Coherent Innova 200 Ar-ion laser pumped Ti:sapphire Coherent 899 ring laser) and the 514.5 nm line (of the same Ar-ion laser) were used, respectively. For resonant excitation of Raman spectrum of the sol system, the 488 nm line of the Ar-ion laser was used to pump a Coherent 599 dye laser, using dichloromethane (DCM), to provide 646 nm radiation. Incident radiation entered at a right angle to the collected Raman scattered light, which was focused onto the entrance slit of a 0.6 m Spex 1877 Triplemate grating spectrometer, with the 1200 grooves/mm grating selected, and then imaged onto a Spex Spectrum-1 liquid-nitrogen-cooled, charge-coupled device (CCD) detector.

Calculations. The ground-state geometry of the DDPT was optimized without symmetry restriction on the initial structure. Both structure optimization and vibrational analysis calculations were implemented using DFT with functionals,[13] specifically, B3LYP, in which the exchange functional is of the Becke's three-parameter type, including gradient correction,[14] and the correlation correction involves the gradient-corrected functional of Lee, Yang, and Parr.[15] The basis set of split valence type 6-31G(d),[16] as contained in the Gaussian 98 software package,[17] was used. The vibrational-mode descriptions were made based on calculated nuclear displacements and relative intensities associated with measured vibrational frequencies and intensities, combined with visual inspection of the animated normal modes, to assess which bond and angle motions dominate the mode dynamics attributed to a particular vibrational band for the molecule.

III. Results and Discussion

Structure. The structure and atomic labeling of the DDPT molecule are depicted in Figure 2. The DFT method at the B3LYP/6-31G(d) level indicates that, as mentioned, there are two possible low-energy geometric structures (see Figures 3A and B) for the gas-phase species. The most stable of these structures is not quite planar, with the two planar benzothiazole moieties twisted by 14.4°, with respect to each other; the ethyl groups point in the opposite direction from the phenyl group on the methine change, whereas the methyl groups of the ethyl substituents are positioned on opposite sides of the structural surface of the macrocycle (see Figure 3A). Hereinafter, we refer to this structure as the trans configuration. The second favorable

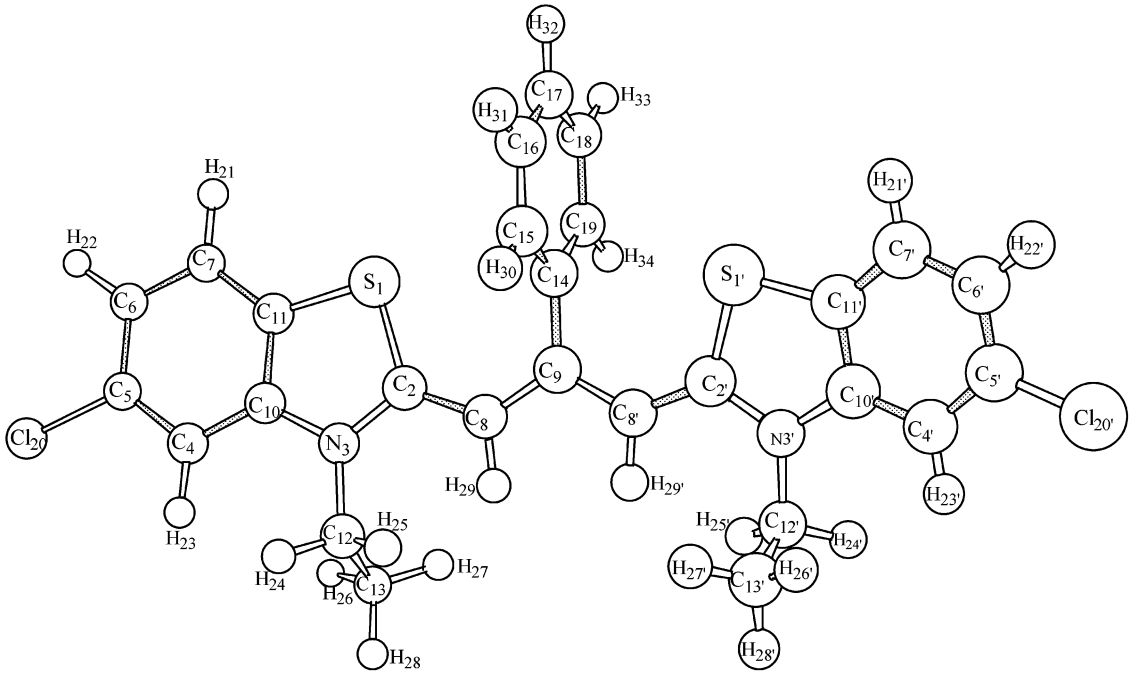

Figure 2. Structure and atomic labeling of the DDPT molecule.

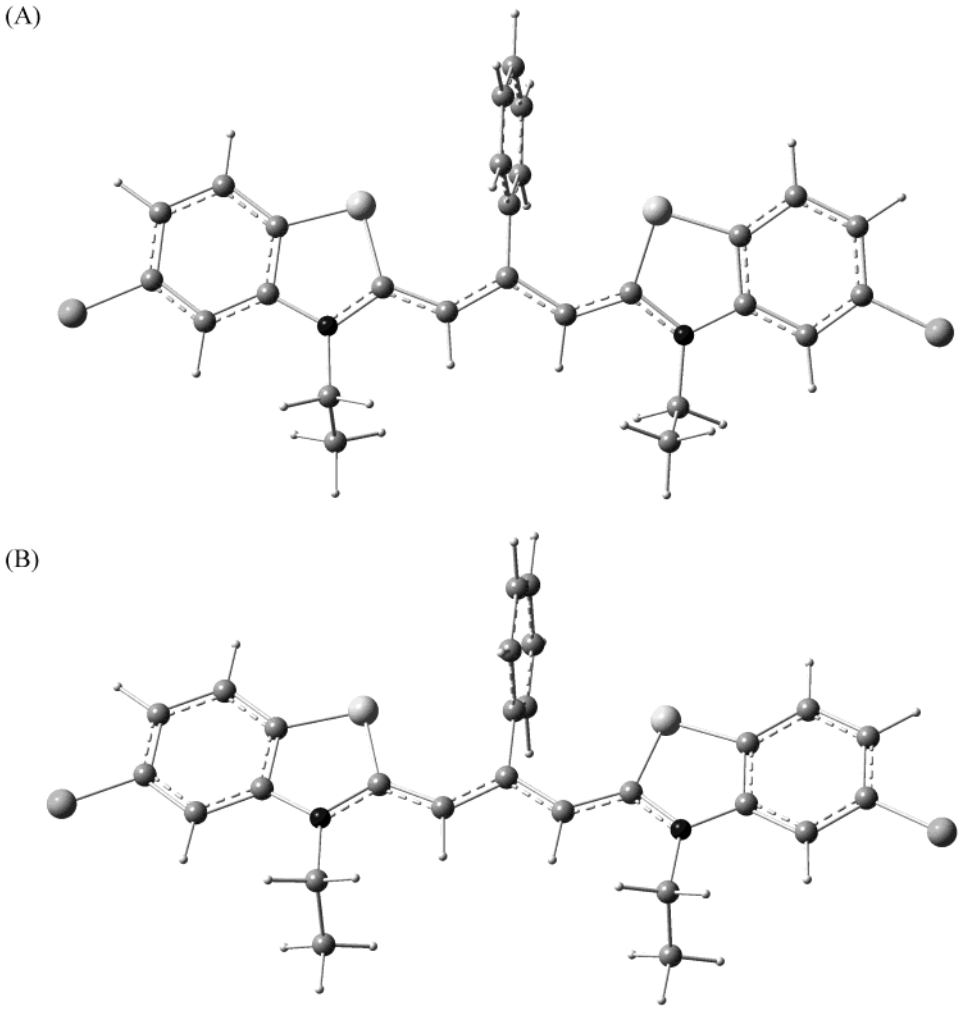

Figure 3. Low-energy geometrical structures of DDPT, calculated by the DFT method at the B3LYP/6-31G(d) level ((A) trans conformer and (B) cis conformer).

structure is planar (see Figure 3B), with the methyl groups lying on the same side of the surface of the macrocycle (i.e., the cis conformer). In both cases, the methyl groups are approximately perpendicular to the structural surface of the macrocycle, and the phenyl rings on the respective methine bridges make angles of 83.4° and 89.7° for the trans and cis conformers, relative to the structural surface of the macrocycle. Calculations indicate that the cis configuration lies only 107 cm^{-1} above the energy of the trans conformer; therefore, both structures are likely populated at room temperature.

The molecular structure of the DDPT is similar to that of 3,3′-diethylthiacarbocyanine (DTCC), for which, in 1959, Wheatley studied the molecular structures of the solvated DTCC-bromide crystals[18] and nonsolvated DTCC-bromide crystals,[19] using X-ray single-crystal methods. In those studies, it was determined that, despite very close molecular dimensions of the cation, the molecular and crystal structures of the solvated and nonsolvated molecules were different. In particular, the nonsolvated cation was determined to be planar, with the methyl groups of the ethyl substituents lying on the same side of the cationic plane; the solvated form deviated somewhat from being planar, with the two benzothiazole moieties twisted through an angle of 8°, with respect to each other, whereas the methyl groups of the ethyl substituents were determined to be on opposite sides of the cationic plane.

The nonplanarity of the solvated cation was not attributed to interaction with the ethanol solvate, because there were no short contacts between the solvent and the atoms of the cationic plane that might account for the departure of the cation from planarity, as a result of packing forces.[19] The experimentally determined molecular structures of the solvated and nonsolvated form of the DTCC cation are consistent with those predicted for the two molecular structures of DDPT calculated using the DFT method reported herein.

Tables 1−3 provide predicted bond distances and angles for gas-phase DDPT, as well as measured values of bonds and angles for the DTCC cation. For the latter, the bond length for the nonsolvated species is reported to have a precision of ∼0.1Å.[18] The predicted values of the bond lengths and angles of the DDPT cation are in good agreement with X-ray measurements for both the solvated and nonsolvated forms of DTCC. (Note that, in the tables, measured values for DTCC are provided in the "solvated/nonsolvated" format.)

The average C−C bond length of the trimethine bridge is 1.4033 Å (1.424 Å/1.455 Å), and the 18 bonds of the phenyl groups average 1.3978 Å (1.397 Å/1.472 Å). The average value of the N−C bonds of the cation is 1.3705 Å (1.405 Å/1.375 Å) for the conjugated N_3-C_2-type bonds, 1.4006 Å (1.41 Å/1.395 Å) for N_3-C_{10}-type bonds, and 1.4748 Å (1.485 Å/1.535 Å) for the nonconjugated N_3-C_{12}-type bonds. These values are consistent with the well-known values of 1.34 Å for atomic N−C bonds and 1.47 Å for nonconjugated N−C bonds. In addition, the C−C bonds of the ethyl groups average 1.5298 Å (1.53 Å/1.54 Å); the predicted $C_{11}-S_1$ and S_1-C_2 bonds are,

TABLE 1: DDPT Bond Lengths:[a] Calculated and Experimental

bond	bond length (Å)			
	trans-DDPT	A[b]	cis-DDPT	B[c]
$S_1C_2/S_{1'}C_{2'}$	1.7610	1.79/1.78	1.7609	1.81/1.74
$S_1C_{11}/S_{1'}C_{11'}$	1.7582	1.73/1.77	1.7581	1.73/1.79
$C_2N_3/C_{2'}N_{3'}$	1.3705	1.43/1.38	1.3708	1.40/1.35
$N_3C_{10}/N_{3'}C_{10'}$	1.4006	1.41/1.41	1.4007	1.38/1.41
$N_3C_{12}/N_{3'}C_{12'}$	1.4748	1.48/1.49	1.4748	1.55/1.52
$C_4C_{10}/C_{4'}C_{10'}$	1.3982	1.39/1.41	1.3983	1.49/1.49
$C_5C_4/C_{5'}C_{4'}$	1.3936	1.40/1.42	1.3935	1.45/1.47
$C_5C_6/C_{5'}C_{6'}$	1.4014	1.41/1.41	1.4014	1.51/1.42
$C_6C_7/C_{6'}C_{7'}$	1.3923	1.39/1.39	1.3923	1.52/1.45
$C_7C_{11}/C_{7'}C_{11'}$	1.3934	1.39/1.38	1.3934	1.45/1.44
$C_{10}C_{11}/C_{10'}C_{11'}$	1.4015	1.41/1.42	1.4014	1.49/1.44
$C_2C_8/C_{2'}C_{8'}$	1.4019	1.41/1.45	1.4018	1.45/1.46
$C_8C_9/C_9C_{8'}$	1.4060	1.43/1.41	1.4060	1.45/1.46
$C_{12}C_{13}/C_{12'}C_{13'}$	1.5298	1.52/1.54	1.5297	1.54/1.54
C_9C_{14}	1.4947		1.4952	
$C_{17}C_{16}/C_{18}C_{17}$	1.3970		1.3971	
$C_{16}C_{15}/C_{19}C_{18}$	1.3946		1.3943	
$C_{14}C_{15}/C_{14}C_{19}$	1.4048		1.4046	
$C_5Cl_{20}/C_{5'}Cl_{20'}$	1.7469		1.7469	
$C_4H_{23}/C_{4'}H_{23'}$	1.0827		1.0827	
$C_6H_{22}/C_{6'}H_{22'}$	1.0839		1.0839	
$C_7H_{21}/C_{7'}H_{21'}$	1.0852		1.0852	
$C_8H_{29}/C_{8'}H_{29'}$	1.0846		1.0846	
$C_{12}H_{25}/C_{12'}H_{25'}$	1.0917		1.0917	
$C_{12}H_{24}/C_{12'}H_{24'}$	1.0923		1.0922	
$C_{13}H_{27}/C_{13'}H_{27'}$	1.0945		1.0945	
$C_{13}H_{26}/C_{13'}H_{26'}$	1.0942		1.0942	
$C_{13}H_{28}/C_{13'}H_{28'}$	1.0947		1.0947	
$C_{15}H_{30}/C_{19}H_{34}$	1.0865		1.0864	
$C_{16}H_{31}/C_{18}H_{32}$	1.0861		1.0861	
$C_{17}H_{32}$	1.0861		1.0861	

[a] The designations trans- and cis- refer to the relative positions of the methyl groups on the ethyl substituents. The prefix "trans-" indicates that the methyl groups lie on opposite sides of the DDPT cation structural surface, whereas "cis-" indicates that they lie on the same side. The bond lengths shown have been calculated using the B3LYP/6-31G(d) level of theory. [b] Measured bond lengths of the 3,3′-diethyl thiacarbocyanine cation for the methanol solvated form (see ref 19). [c] Measured bond lengths of the 3,3′-diethyl thiacarbocyanine cation for the methanol unsolvated form (see ref 18). The uncertainty in the bond length is 0.1 Å.

TABLE 2: Bond Angles of trans- and cis-DDPT[a]

bond angle	value (deg)		
	trans-DDPT	cis-DDPT	Θ[b]
$C_6-C_5-C_4/C_{6'}-C_{5'}-C_{4'}$	122.1	122.1	119/119
$C_6-C_5-Cl_{20}/C_{6'}-C_{5'}-Cl_{20'}$	119.2	119.2	
$C_4-C_5-Cl_{20}/C_{4'}-C_{5'}-Cl_{20'}$	118.7	118.7	
$C_5-C_6-C_7/C_{5'}-C_{6'}-C_{7'}$	119.8	119.8	124/118
$C_5-C_6-H_{22}/C_5-C_6-H_{22'}$	119.8	119.8	
$C_6-C_7-C_{11}/C_{6'}-C_{7'}-C_{11'}$	118.7	118.7	119/122
$C_6-C_7-H_{21}/C_{6'}-C_{7'}-H_{21'}$	120.3	120.3	
$C_7-C_{11}-C_{10}/C_{7'}-C_{11'}-C_{10'}$	121.1	121.1	114/119
$C_{10}-C_{11}-S_1/C_{10'}-C_{11'}-S_{1'}$	110.8	110.8	119/113
$C_{11}-C_{10}-C_4/C_{11'}-C_{10'}-C_{4'}$	120.6	120.6	129/120
$C_{11}-C_{10}-N_3/C_{11'}-C_{10'}-N_{3'}$	112.4	112.4	105/110
$C_5-C_4-C_{10}/C_{5'}-C_{4'}-C_{10'}$	117.6	117.6	114/121
$C_5-C_4-H_{23}/C_{5'}-C_{4'}-H_{23'}$	119.9	119.8	
$C_{11}-S_1-C_2/C_{11'}-S_{1'}-C_{2'}$	91.2	91.2	88/89
$S_1-C_2-N_3/S_{1'}-C_{2'}-N_{3'}$	110.6	110.6	109/111
$S_1-C_2-C_8/S_{1'}-C_{2'}-C_{8'}$	126.3	126.3	127/129
$N_3-C_2-C_8/N_{3'}-C_{2'}-C_{8'}$	123.1	123.1	122/120
$C_{10}-N_3-C_{12}/C_{10'}-N_{3'}-C_{12'}$	121.3	121.2	124/127
$C_{10}-N_3-C_2/C_{10'}-N_{3'}-C_{2'}$	115.0	115.0	117/116
$C_{12}-N_3-C_2/C_{12'}-N_{3'}-C_{2'}$	123.8	123.8	118/117
$C_2-C_8-C_9/C_{2'}-C_{8'}-C_{9'}$	129.3	129.4	115/118
$N_3-C_{12}-C_{13}/N_{3'}-C_{12'}-C_{13'}$	113.1	113.1	102/98
$C_8-C_9-C_{14}/C_{8'}-C_9-C_{14}$	121.0	121.0	
$C_9-C_{14}-C_{15}/C_9-C_{14}-C_{19}$	120.3	120.2	
$C_8-C_9-C_{8'}$	118.0	117.9	
$C_{15}-C_{14}-C_{19}/C_{16}-C_{17}-C_{18}$	119.4/120.0	119.4	
$C_{14}-C_{15}-C_{16}/C_{14}-C_{19}-C_{18}$	120.2	120.2	
$C_{15}-C_{16}-C_{17}/C_{19}-C_{18}-C_{17}$	120.1	120.1	
$C_{14}-C_{15}-H_{30}/C_{14}-C_{19}-H_{34}$	119.7	119.6	
$C_{15}-C_{16}-H_{31}/C_{19}-C_{18}-H_{33}$	119.7	119.7	
$C_{16}-C_{17}-H_{32}/C_{18}-C_{17}-H_{32}$	120.0	120.0	

[a] The designations trans- and cis- refer to the relative positions of the methyl groups on the ethyl substituents. The prefix "trans-" indicates that the methyl groups lie on opposite sides of the DDPT cation structural surface, whereas "cis-" indicates that they lie on the same side. The bond lengths shown have been calculated using the B3LYP/6-31G(d) level of theory. [b] Θ is the bond angle for the solvated form of 3,3′-diethylthiacarbocyanine, estimated using the GaussView package program from the orthogonal Cartesian coordinates provided in ref 19.

respectively, 1.7582 Å (1.75 Å/1.76 Å) and 1.7610 Å (1.785 Å/1.775 Å); and the C−Cl bonds average 1.7469 Å, which is in good agreement with the calculated value of 1.7394 Å and the experimental value of 1.737 Å (see the work of Aydin et al.[20] and Smith and Luss,[21] respectively) for the 1,1′,3,3′-tetraethyl-5,5′,6,6′-tetrachlorobenzimidazolocarbocyanine (TTBC) cation.

The average values of the C−S−C and C−N−C bond angles of the thiazole moieties are calculated to be 91.2° (89.5°) and 115° (116°), respectively; the average Cl−C_5−C and Cl−$C_{5'}$-C angle is 119.2°, which is consistent with the calculated value of 117.67° and the measured value of 116.1° for the TTBC cation; and the remaining phenyl angles average 119.6° (119.9°). As mentioned previously and shown in Tables 1 and 2, the calculated bond distances and angles of the DDPT in the gas phase are, to great accuracy, consistent with the single-crystal X-ray diffraction (XRD) values for the DTCC cation (see refs 18 and 19) and the TTBC cation (see ref 21).

Information concerning the potential cause of the twist between the benzothiazole moieties is also provided by the structure calculation. The 14.4° distortion seems to be due to intramolecular steric interaction between H_{29} ($H_{29'}$) and the ethyl group at N_3 ($N_{3'}$) for the trans conformation of the methyl groups of the ethyl substituents. As a result of this spatial proximity, the repulsive interaction between the ethyl groups and hydrogen on the bridge are in opposite directions for the trans conformer and would explain the two benzothiazole moieties being twisted away from each other. For the cis conformer, this repulsive interaction would be in the same direction, which would not result in a twist between the two chromophores. We calculate, additionally, that the average contacts between groups are as follows: 2.530 Å for methylene-H on the trimethine bridge (i.e., $C_{12}\cdots H_{29}$), 7.084 Å for methylene···methylene (i.e., $C_{12}\cdots C_{12'}$), 7.180 Å for methyl···methyl (i.e., $C_{13}\cdots C_{13'}$), and 7.060 Å for methylene···methyl $C_{12}\cdots C_{13'}$ (and $C_{13}\cdots C_{12'}$). The dihedral angles associated with $N_3-C_2-C_8-C_9$, $C_2-C_8-C_9-C_{8'}$, $C_8-C_9-C_{8'}$-$C_{2'}$, and $C_9-C_{8'}$-$C_{2'}$-$N_{3'}$ have the same value of −176.4°.

Charge Distribution. The calculated natural atomic charge distribution of the DDPT cation, using Natural Population Analysis (NPA) at the B3LYP/6-31G(d) level, is given in Table 4. For both conformers, our results indicate that the partial charge distribution of the DDPT cation is symmetrically distributed with respect to the *y*-axis, which passes through the C_9-phenyl bond. The charges among the atoms within the cation are observed to be localized on the thiazole rings, with the S and N atoms and their accompanying conjugated C atoms alternately charged negatively and positively. We find that the net charges on the N atoms are approximately twice that of their adjacent C atoms in the conjugated ring. Also, most of the partial charge among the atoms within the molecule is

TABLE 3: Dihedral Angles of trans- and cis-DDPT[a]

dihedral angle	Value (deg) trans-DDPT	cis-DDPT
$C_4-C_5-C_6-C_7$	0.2	0.2
$C_4-C_5-C_6-H_{22}$	180.0	180.0
$Cl_{20}-C_5-C_6-C_7$	−179.6	−179.6
$C_6-C_7-C_{11}-C_{10}$	−0.4	−0.3
$C_6-C_7-C_{11}-S_1$	179.7	179.5
$C_7-C_{11}-C_{10}-C_4$	0.7	0.7
$C_7-C_{11}-C_{10}-N_3$	−179.1	−179.1
$S_1-C_{11}-C_{10}-C_4$	−179.4	−179.2
$S_1-C_{11}-C_{10}-N_3$	0.8	1.0
$C_{10}-C_{11}-S_1-C_2$	0.3	0.1
$C_{11}-S_1-C_2-C_8$	177.2	178.3
$C_{11}-C_{10}-N_3-C_{12}$	178.4	178.5
$C_2-N_3-C_{12}-C_{13}$	−90.1	−89.4
$N_3-C_2-C_8-H_{29}$	5.3	3.8
$N_3-C_2-C_8-C_9$	−176.4	−176.3
$C_2-C_8-C_9-C_{14}$	3.6	0.1
$C_8-C_9-C_{14}-C_{15}$	83.4	89.7
$C_8-C_9-C_{8'}-C_{2'}$	−176.4	−179.4
$C_9-C_{14}-C_{15}-C_{16}$	179.8	180.0
$C_9-C_{14}-C_{19}-C_{18}$	179.8	−180.0
$C_9-C_{8'}-C_{2'}-N_{3'}$	−176.4	176.3
$C_9-C_{8'}-C_{2'}-S_{1'}$	5.1	−4.3
$C_{2'}-N_{3'}-C_{12'}-C_{13'}$	−90.1	89.4

[a] The designations trans- and cis- refer to the relative positions of the methyl groups on the ethyl substituents. The prefix "trans-" indicates that the methyl groups lie on opposite sides of the DDPT cation structural surface, whereas "cis-" indicates that they lie on the same side. The bond lengths shown have been calculated using the B3LYP/6-31G(d) level of theory.

heavily localized on the C_{10} (0.1614), N_3 (−0.3645), and S_1 (0.5063) atoms in the conjugated ring atoms and on the C_{13} atom (−0.6954) in side chain on the N atom. The remaining C atoms, including those within the trimethine bridge, but not including the methyl carbon, have a relatively small and negative net charge. The Cl atoms have a small amount of net positive charge, relative to their adjacent C atoms. Also, in the trimethine bridge, charge distribution alternates as follows: C_8 (−0.3482), C_9 (0.0672), and $C_{8'}$ (−0.3482); in the phenyl ring on the bridge, the localized charges are small and negative (less than −0.2; see Table 4). The charge distribution generally is not symmetric, with respect to the *x*-axis, leading to the *y*-component of the dipole moment alone differing from zero: $\mu_x = -0.0004$ D, $\mu_y = -1.7209$ D, and $\mu_z = 0.0004$ D, where the *x*-axis is oriented along the long molecular axis, the *y*-axis is oriented along the C_9-phenyl ring on the trimethine bridge, and the *z*-axis is perpendicular to the (*x*,*y*)-plane.

The predicted charge distribution of the cation suggests a structural picture for the aggregate in which the DDPT cations within the aggregate are aligned such that the benzothiazole moieties of adjacent cations have a center-of-inversion relationship between them.

Vibrational Mode Assignments. The observed vibrational bands in the Raman spectrum of the DDPT cation in methanol were assigned based on the density functional prediction at the B3LYP/6-31G(d) level for the gas-phase species. The calculated vibrational frequencies coincided with those observed in the Raman spectrum of DDPT, using a linear factor of 0.973. We used the calculated frequencies and, to some degree, the calculated intensity distribution to attribute observed vibrational frequencies and intensities to specific intramolecular motions of DDPT. These latter assessments were facilitated by analysis of the calculated nuclear displacements, combined with animation of their vibrations, to identify specific motions as the dominant movements within the molecule. This is not a truly rigorous approach but should provide adequate insight. The assignments of the vibrational mode are provided in Table 5, whereas Figure 4 provides the nuclear displacement for several selected vibrational modes. For this latter figure, because the vibrational motions of DDPT are spatially symmetrical, with respect to the phenyl ring on the trimethine bridge, we display nuclear displacements using only half of the DDPT cation.

The nonresonance Raman spectrum of monomeric DDPT exhibits many vibrational bands in the range of 300−1700 cm^{-1}, as shown in Figure 5A. The more-intense Raman bands are observed at 597, 1150, 1237, 1332, and 1442 cm^{-1}; medium-intensity Raman features occur at 871, 1416, 1471, 1553, and 1579 cm^{-1}, and many relatively weak peaks are dispersed

TABLE 4: Calculated Natural Atomic Charges and Dipole Moments of the DDPT Cation,[a] at the B3LYP/6-31G(d) Level

	trans-DDPT	cis-DDPT
Atomic Charge, Thiacarbocyanine		
S_1, $S_{1'}$	0.5063	0.5065
C_2, $C_{2'}$	0.0884	0.0881
N_3, $N_{3'}$	−0.3645	−0.3645
C_4, $C_{4'}$	−0.2706	−0.2706
C_5, $C_{5'}$	−0.0316	−0.0315
C_6, $C_{6'}$	−0.2332	−0.2332
C_7, $C_{7'}$	−0.2104	−0.2104
C_8, $C_{8'}$	−0.3482	−0.3473
C_{10}, $C_{10'}$	0.1614	0.1615
C_{11}, $C_{11'}$	−0.2324	−0.2324
C_{12}, $C_{12'}$	−0.2627	−0.2621
C_{13}, $C_{13'}$	−0.6954	−0.6954
Cl_{20}, $Cl_{20'}$	0.0402	0.0402
H_{21}, $H_{21'}$	0.2636	0.2643
H_{22}, $H_{22'}$	0.2715	0.2715
H_{23}, $H_{23'}$	0.2644	0.2636
H_{24}, $H_{24'}$	0.2574	0.2573
H_{25}, $H_{25'}$	0.2519	0.2511
H_{26}, $H_{26'}$	0.2480	0.2480
H_{27}, $H_{27'}$	0.2398	0.2402
H_{28}, $H_{28'}$	0.2558	0.2557
H_{29}, $H_{29'}$	0.2434	0.2430
Atomic Charge, Phenyl Group		
C_9	0.0672	0.0673
C_{14}	−0.1314	−0.1314
C_{15}	−0.2137	−0.2118
C_{16}	−0.2219	−0.2210
C_{17}	−0.2144	−0.2150
C_{18}	−0.2219	−0.2226
C_{19}	−0.2137	−0.2163
H_{30}	0.2524	0.2526
H_{31}	0.2531	0.2531
H_{32}	0.2526	0.2529
H_{33}	0.2531	0.2520
H_{34}	0.2524	0.2531
H_{33}	0.0672	0.0673
H_{34}	−0.1314	−0.1314
Dipole Moment[b]		
μ_x	−0.0004 D	−0.0001 D
μ_y	−1.7209 D	−1.7317 D
μ_z	0.0004 D	−0.2077 D
μ_{tot}	1.7209 D	1.7441 D

[a] The designations trans- and cis- refer to the relative positions of the methyl groups on the ethyl substituents. The prefix "trans-" indicates that the methyl groups lie on opposite sides of the DDPT cation structural surface, whereas "cis-" indicates that they lie on the same side. The bond lengths shown have been calculated using the B3LYP/6-31G(d) level of theory. [b] For the calculated dipole moments, the molecular coordinates are defined as follows: *x*-direction, along the long molecular axis; *y*-direction, along the axis passing through the C_9-phenyl bond; and *z*-direction, perpendicular to the (*x*,*y*)-plane.

TABLE 5: Vibrational Raman Band Assigned to Motions Associated with Normal Vibrational Modes of DDPT

$\Delta\bar{\nu}^{calc}$ (cm^{-1})			$\Delta\bar{\nu}^{meas}$ (cm^{-1})		
unscaled	scaled[a]	intensity (Å^4/amu)	monomer[b]	aggregate[c]	assignment[d]
134.5	130.9	0.8		142	τ_{op}(Q)/w_{op}(Brd)
198.0	192.7	2.5		161	τ_{op}(Q)/w_{op}(Brd)/ρ(ethyl, C_2H_5)
224.1	218.0	2.7		212	w_{op}(bridge Ph)/ρ(methyl, CH_3)
252.7	245.9	5.1		250	w_{op}(Brd)/δ_{op}(Q)/ρ(ethyl)
283.0	275.4	4.6		274	δ_{op}(Q)/w_{op}(Brd)/ρ(ethyl)
375.1	364.9	25.4		365	R_{ip}(half-Ph)/ρ(ethyl)
445.6	433.6	7.1		440	δ_{op}(bridge Ph)/w(Brd)/ρ(methylene, CH_2)
483.0	469.9	10.6	471	471	R_{ip}(Q)/r(CH_2)/weak w(Brd)
613.4	596.9	65.9	598	598	τ_{op}(Q)/r(CH_2)/$w_{op}(CH)_{Brd}$
739.5	719.6	13.7	714	714	δ_{ip}(Q)/w(CH_2)
879.7	856.0	87.8	870	870	ρ(ethyl)/τ_{ip}(Q)/$\beta(CH)_{Brd}$
1151.3	1120.3	726.7	1125	1125	δ_{ip}(half-bridge Ph)/ν($C_8C_9C_{8'}$, Brd)/ρ(ethyl)/$\beta(CH)_{Ph\ at\ Brd}$
1174.7	1143.0	2072.5	1150	1150	δ_{ip}(bridge Ph)/ν(Brd)/ρ(ethyl)/weak δ_{ip}(Ph)/δ_{as}(Py)
1267.5	1233.3	3197.6	1237	1237	ρ(ethyl)/w(C_nH, n=4 and 7)/β(Brd)/weak δ_{ip}(Q)
1296.7	1261.7	501.6	1260	1260	$\beta(CH)_{Ph+Brd}$/τ(CH_2)/weak δ_{ip}(Q)
1402.0	1364.2	1057.7	1332	1332	w_{op}(CH_2)/$\beta(CH)_{Brd}$/weak δ_{ip}(Q)
1451.5	1412.3	249.7	1416	1416	β(Brd)/weak δ_{ip}(half-bridge Ph.)/$\beta(CH)_{Ph-Brd}$/weak ρ(methyl)
1474.6	1434.8	3450.0	1441	1441	$\delta_{ip,as}$(Q)/$\beta(CH)_{Ph}$/τ(methylene)
1509.0	1468.3	827.0	1471	1471	δ_{ip}(Ph)/weak δ_{ip}(Py)/$\beta(CH)_{Ph}$
1539.6	1498.1	3023.8	1504	1504	ν_{as}($C_8C_9C_{8'}$, Brd)/ρ(ethyl)/$\beta(CH)_{Brd}$
1600.9	1557.7	3305.3	1553	1553	ν_{as}(NC_2C_8)/β(Brd)/$\beta(CH)_{Brd}$/ρ(CH, in CH_2)
1622.4	1578.6	2353.0	1579	1579	δ_{ip}(Ph)/δ_{ip}(Py, half-ring)/$\beta(CH)_{Ph}$
1638.8	1594.5	149.6	1607	1607	δ_{ip}(Ph)

[a] The scaling factor used was 0.975. [b] Off-resonance Raman analysis of the monomeric species was acquired using 705 nm excitation. [c] Resonance Raman analysis of the aggregate was acquired using 646 nm excitation. [d] The identifications of specific motions of DDPT are represented by the following: δ, deformation; R, rotation; ν, stretching; ρ, rocking; w, wagging; τ, twisting; β, bending; ip, in-plane; op, out-of-plane; Ph, conjugated phenyl moieties; Py, thiazole moieties; Q, benzothiazole macrocycle (conjugated phenyl plus thiazole moieties); Brd, trimethine bridge; and as, asymmetric stretch.

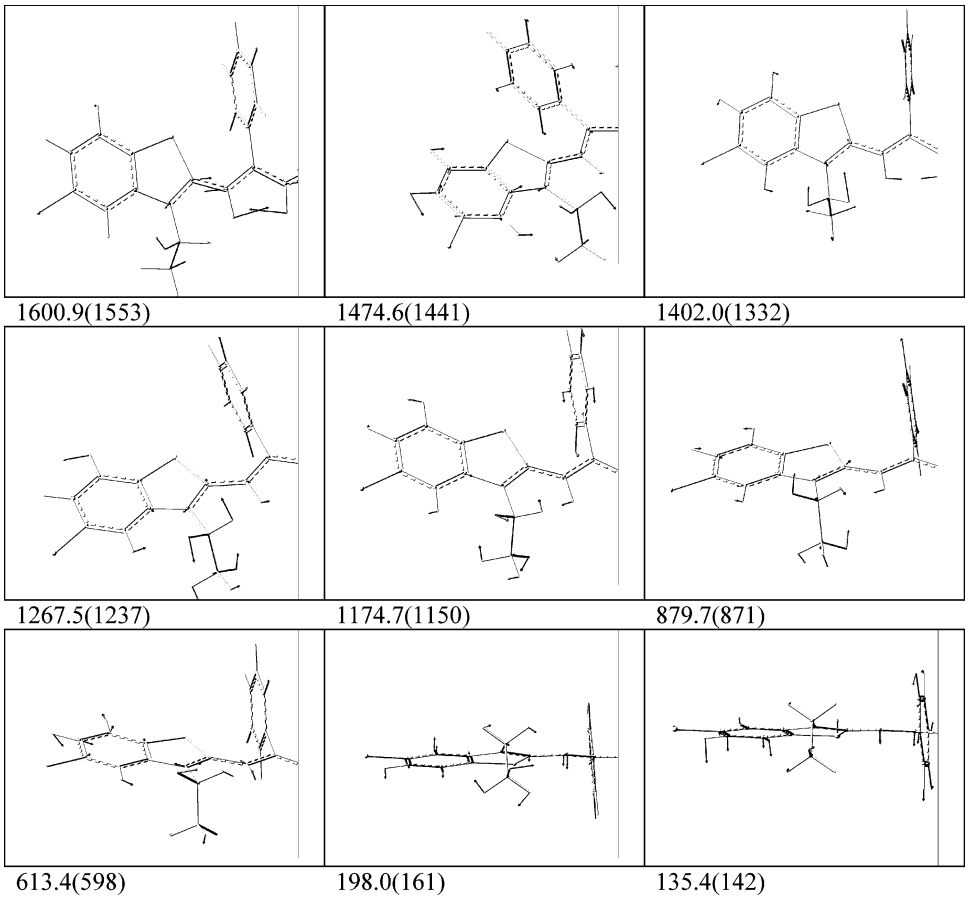

Figure 4. Calculated relative normal mode displacements for DDPT, as determined using the B3LYP/6-31G(d) level of theory. Only the motion of half of the cation is provided, because the other half undergoes the same movements.

throughout the spectrum. The calculations, coupled with the animated motions, suggest that the observed Raman vibrational modes of monomeric DDPT are due to symmetric and asymmetric skeletal deformations of the benzothiazole ring, combined with distortions of the trimethine bridge, as well as with rocking and wagging of the CH bonds in the phenyl central group.

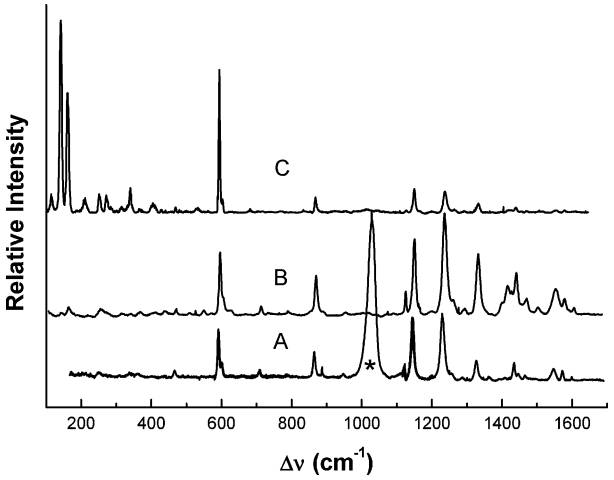

Figure 5. Raman spectra of monomeric and aggregated DDPT. Spectrum A shows the nonresonant excitation of the monomer in a methanol solution, using 705 nm radiation; the laser power is 300 mW at the source, the accumulation time is 12 min, and the spectral resolution is 0.4 nm. (The broad intensity band at ca. 1000 cm^{-1}, labeled by an asterisk (*), is due to the solvent.) Spectrum B shows the nonresonant excitation of an aggregate adsorbed onto aqueous silver sol particles excited using 514.5 nm radiation; the laser power is 25 mW at the source, the accumulation time is 2 min, and the spectral resolution is 0.4 nm. Spectrum C shows the resonance Raman spectrum of same system as spectrum B, excited using 646 nm radiation; the laser power is 12 mW at the source, the accumulation time is 6 s, and the spectral resolution is 0.4 nm.

Observed Vibrational Bands of Aggregated DDPT. There are several Raman bands of the DDPT cation whose decompositions into principal motions may provide high-resolution insight into intermolecular alignments of monomers within the aggregate structure. One method to make these special bands stand out from other bands is the comparison of Raman spectra for DDPT existing as the isolated monomer versus those intercalated within the aggregate. Further insight is gained by observing changes in the Raman spectra of aggregated DDPT under both nonresonant and resonant excitation conditions. For nonresonant excitation, earlier studies from this laboratory have been interpreted as indicating that the Raman spectrum should emphasize the constricted environmental (or site) influence on vibrations, whereas the use of resonant excitation should identify bands whose motions have major components in the aggregate formation direction that should favor coupling between the motion of the exciton and charge oscillations associated with the vibrations.

Figure 5 shows Raman spectra of monomeric and aggregated DDPT with excitation at nonresonant wavelengths (see Figures 5A and B, respectively). Comparison of the spectral patterns in these cases indicates that no significant shifts in spectral positions occur for any bands. However, significant differences in the relative intensities are observed for many bands. For example, Figure 5B, when compared to Figure 5A, indicates changes in the higher-frequency region (associated with in-plane or very little motion of the macrocycle). The bands at 1332 and 1441 cm^{-1}, as indicated in Table 5, involve in-plane deformation (δ) of the macrocycle, as well as component motions that involve the methyl group within the ethyl attached to the benzothiazole moiety or phenyl group motions. Thus, vibrations that involve the benzothiazole seem to be enhanced when the molecule is part of the aggregate, even when nonresonant excitation is used. This is to be expected, because $\pi-\pi^*$ interactions between aromatic chromophores are expected to have dominant roles in holding the aggregate together. In addition, the motions of the aromatic groups, even when in-plane, are expected to be amplified through induced electronic distribution changes in adjacent aromatic chromophores, leading to increased polarizability of the aggregate structure and enhanced Raman scattering.

With resonant excitation (see Figure 5C), three bands are observed to be significantly affected. One of these bands, the isolated band at ca. 598 cm^{-1}, involves twisting of the macrocycle (i.e., $\tau_{op}(Q)$), as well as rocking of the ethyl CH_2 (i.e., $\rho(CH_2)$) and out-of-plane wagging (i.e., $w_{op}(CH)_{Brd}$) of the CH in the methane bridge (see Table 5). The other two bands that are dramatically enhanced with resonance excitation are those at 142 and 161 cm^{-1}. The Raman band at 142 cm^{-1} is assigned to out-of-plane twisting of the benzothiazole moieties (i.e., $\tau_{op}(Q)$), accompanied by out-of-plane wagging of the bridge. The Raman feature at 161 cm^{-1} is attributed to out-of-plane twisting of the benzothiazole moieties (i.e., $\tau_{op}(Q)$), combined with out-of-plane wagging of the trimethine bridge (i.e., $w_{op}(Brd)$) and rocking of the ethyl group (i.e., $\rho(ethyl)$). As mentioned previously, the motion that dominates in both is the out-of-plane distortion of the macrocycle. This determination is consonant with the expectation that resonant excitation should identify bands whose motions have major components in the aggregate formation direction. Phenomena quite similar to those described previously have been addressed in several earlier papers from this laboratory that have focused on the so-called "aggregation-enhanced scattering" (AERS) theory,[22−24] which utilizes Herzberg−Teller intensity borrowing, as developed by Albrecht.[25] In these publications, one of us (D.L.A.) has shown that the enhancement of Raman bands for aggregated molecules is mainly attributable to the existence of molecular exciton states and the concomitant enhanced polarizability of the aggregate structure. The Raman intensity, which is proportional to the square of the polarizability (α), can be decomposed into three terms, as follows:

$$\alpha_{ij}^{gv',gv''} = A + B + C$$

where i and j represent the polarization directions, g indicates the ground electronic state, and v′ and v″ refer to upper and lower vibrational states. The *C* term, as has been shown earlier,[24] is expected to be less important than the *A* or *B* terms. In summary, the AERS formulation attributes bands that show substantial intensity enhancement upon use of resonance excitation as being due to nonvanishing matrix elements that involve excited-state lattice phonon modes of the aggregate, resulting from the intermolecular potential function, and intramolecular modes (i.e., *A*-term bands). Also, Raman bands that are present when either nonresonant or resonant excitation is used are *B*-term bands, and are likely fundamentals, because, with nonresonant excitation, these same modes, as a result of closure over excited-state modes, must be fundamentals in the harmonic oscillator approximation.[26]

The Structure of the Aggregate. The arrangement of DDPT monomers within the aggregate can be inferred from the charge distribution and Raman bands that are enhanced when the aggregate is formed. The monomer's arrangement is reasonably envisioned as having the methyl group of the ethyl substituent, assuming a minimal interaction with the phenyl ring on the trimethine bridge. Such an arrangement can occur when the DDPT monomers assume a staircase, shifted-deck-of-cards alignment, allowing for minimum repulsive interaction. This model is also supported by the predicted charge distribution within the single molecule, where the charge is mostly localized on the thiazole moiety. The permanent dipoles would be aligned

in parallel in this picture; however, the transition dipole, which is calculated using time-dependent functional theory (DT-DFT) at the B3LYP/6-316d level, is determined to have components, relative to the center of each monomer, that lead to the *x*-component of the transition dipole moment alone differing substantially from zero: $\mu_x = 4.7181$ D, $\mu_y = 0.0000$ D, and $\mu_z = 0.0328$ D (where the *x*-axis is oriented along the long molecular axis, the *y*-axis is oriented along the C_9-phenyl ring on the trimethine bridge, and the *z*-axis is perpendicular to the (*x*,*y*)-plane. The alignment of transition dipole, as a result, would be head-to-tail, corresponding to the alignment that defines the so-called J-aggregate structure.

IV. Conclusion

We have coupled theoretical methods with Raman scattering experiments that enable us to give some insight into aggregation of the 3,3′-diethyl-5,5′-dichloro-9-benzothiacarbocyanine (DDPT) cation. The density functional theory (DFT) method, at the B3LYP/6-31G(d) level, indicates that there are two favorable ground-state molecular structures for the DDPT cation, as determined by the relative positions of the methyl groups of the ethyl substituents, relative to the surface defined by the macrocycle chromophore. One of these conformers has a trans arrangement of the methyl groups, resulting in the groups protruding in opposite directions from the surface, whereas the other conformer (i.e., the cis conformer) has the methyl groups on the same side of the macrocycle's surface. The cis conformer is observed to be planar, whereas the trans conformer is twisted, at an angle of 14.4° between two benzothiazole moieties. In addition, the angle between the benzothiazole moieties and the phenyl group at the trimethine bridge is 83.4° for the trans conformer and 89.7° for the cis conformer. The lowest equilibrium ground-state energy of the cis conformer is observed to lie 107 cm^{-1} above the trans conformer.

The arrangement of monomers within the aggregate seems to be described by the traditional spread-deck-of-cards model, which results in essentially parallel permanent dipole moments and a head-to-tail alignment of the transition dipole, leading to the so-called J-aggregate structural picture.

Acknowledgment. D.L.A. thanks the NSF and DoD−ARO for support of this work, in part, through the following awards: (1) the NSF-IGERT Program, under Grant No. DGE-9972892; (2) the NSF-MRSEC Program, under Grant No. DMR-0213574; and (3) DoD−ARO, under Cooperative Agreement DAAD19-01-1-0759.

References and Notes

(1) Pearlstein, R. M. In *Photosynthesis*; Amesz, J., Ed.; Elsevier: Amsterdam, 1987; pp 299−317.

(2) Warshel, A.; Parson, W. W. *J. Am. Chem. Soc.* **1987**, *109*, 6143.

(3) Creighton, S.; Hwang, J.-K.; Warshel, A.; Parson, W. W.; Norris, J. *Biochemistry* **1988**, *27*, 774.

(4) Michel-Beyerle, M. E.; Plato, M.; Deisenhofer, J.; Michel, H.; Bixon, M.; Jorter, L. *Biochim. Biophys. Acta* **1988**, *932*, 52.

(5) Gilman, P. B. *Photogr. Sci. Eng.* **1974**, *18*, 418.

(6) Borsenberger, P. M.; Chowdry, A.; Hoesterey, D. C.; Mey, W. J. *Appl. Phys.* **1978**, *44*, 5555.

(7) Waggoner, A. J. *J. Membr. Biol.* **1976**, *27*, 317.

(8) Krieg, M.; Bilitz, J. M.; Srichai, M. B.; Reymond, R. W. *Biochim. Biophys. Acta* **1994**, *149*, 1199.

(9) Smiley, S.; Reers, M.; Mottola-Hartshorn, C.; Lin, M.; Chen, A.; Smith, T. W.; Steele, G. D., Jr.; Chen, L. B. *Proc. Natl. Acad. Sci., U.S.A.* **1991**, *88*, 3671.

(10) Wang, Y. *J. Opt. Soc. Am. B* **1991**, *8*, 981.

(11) Guo, C.; Aydin, M.; Zhu, H.-R.; Akins, D. L. *J. Phys. Chem. B* **2002**, *106*, 5447.

(12) Creighton, J. A.; Blatchford, C. G.; Albrecht, M. G. *J. Chem. Soc., Faraday Trans. 2* **1979**, *75*, 790.

(13) Bartolotti, L. J.; Flurchick, K. M. In *Reviews in Computational Chemistry, Vol. 7*; Lipkowitz, K. B.; Boyd, D. B., Eds.; VCH Publishers, Inc.: New York, 1996; Chapter 4.

(14) Becke, A. D. *Phys. Rev. A* **1988**, *38*, 3098.

(15) Lee, C.; Yang, W.; Parr, R. G. *Phys. Rev. B* **1993**, *37*, 785.

(16) Gordon, M. S. *Chem. Phys. Lett.* **1980**, *76*, 163.

(17) Frisch, M. J.; Trucks, G. W.; Schlegel, H. B.; Scuseria, G. E.; Robb, M. A.; Cheeseman, J. R.; Zakrzewski, V. G.; Montgomery, J. A., Jr.; Stratmann, R. E.; Burant, J. C.; Dapprich, S.; Millam, J. M.; Daniels, A. D.; Kudin, K. N.; Strain, M. C.; Farkas, O.; Tomasi, J.; Barone, V.; Cossi, M.; Cammi, R.; Mennucci, B.; Pomelli, C.; Adamo, C.; Clifford, S.; Ochterski, J.; Petersson, G. A.; Ayala, P. Y.; Cui, Q.; Morokuma, K.; Malick, D. K.; Rabuck, A. D.; Raghavachari, K.; Foresman, J. B.; Cioslowski, J.; Ortiz, J. V.; Stefanov, B. B.; Liu, G.; Liashenko, A.; Piskorz, P.; Komaromi, I.; Gomperts, R.; Martin, R. L.; Fox, D. J.; Keith, T.; Al-Laham, M. A.; Peng, C. Y.; Nanayakkara, A.; Gonzalez, C.; Challacombe, M.; Gill, P. M. W.; Johnson, B. G.; Chen, W.; Wong, M. W.; Andres, J. L.; Head-Gordon, M.; Replogle, E. S.; Pople, J. A. *Gaussian 98*, revision A.7; Gaussian, Inc.: Pittsburgh, PA, 1998.

(18) Wheatley, P. J. *J. Chem. Soc.* **1959**, 4096.

(19) Wheatley, P. J. *J. Chem. Soc.* **1959**, 3245.

(20) Aydin, M.; Mercier, P.; Stevens, N.; Akins, D. Density Functional and Raman Scattering Study for Structure and Vibrational Mode Analysis of TTBC and Its Aggregate, manuscript in preparation.

(21) Smith, D. L.; Luss, H. R. *Acta Crystallogr., Sect. B: Struct. Crystallogr. Cryst. Chem.* **1972**, *28*, 2793.

(22) Akins, D. L. *J. Phys. Chem.* **1986**, *90*, 1530.

(23) Akins, D. L.; Macklin, J. W. *J. Phys. Chem.* **1989**, *93*, 5999.

(24) Akins, D. L.; Akpabli, C.; Li, X. *J. Phys. Chem.* **1989**, *93*, 1977.

(25) Albrecht, A. C. *J. Chem. Phys.* **1961**, *34*, 1476.

(26) El-Azhary, A. A.; Suter, H. U.; Kubelka, J. *J. Phys. Chem. A* **1998**, *102*, 620.